AIAA Atmospheric Flight Mechanics Conference and Exhibit
21 - 24 August 2006, Keystone, Colorado

AIAA 2006-6276

An Evaluation of Ballute Entry Systems for Lunar Return Missions

Ian G. Clark*, Robert D. Braun†, John Theisinger*, Grant Wells*
Space Systems Design Lab
Guggenheim School of Aerospace Engineering
Georgia Institute of Technology, Atlanta, GA, 30332-0150
ian_clark@ae.gatech.edu

This study investigates the advantages and feasibility of using ballutes for Earth entry at lunar return velocities. Using analysis methods suitable for conceptual design and assuming a CEV type entry vehicle, multiple entry strategies were investigated. Entries that jettison the ballute after achieving low Earth orbit conditions were shown to reduce heating rates to within reusable thermal protection system limits. Deceleration was mitigated to approximately four g's when a moderate amount of lift was applied subsequent to ballute jettison. Primary ballute size drivers are the thermal limitations and areal densities of the ballute material. Performance requirements for both of those metrics were generated over a range of total ballute system masses. Lastly, preliminary investigation of a lower mass cargo variant of the CEV allowed for additional reduction of ballute system mass. However, ballute system mass as a percentage of the total entry mass was shown to be relatively independent of the entry mass.

Nomenclature

C_D	=	drag coefficient
C_p	=	pressure coefficient
D_b	=	ballute diameter, m
D_c	=	diameter of entry vehicle, m
g_0	=	acceleration at Earth's surface due to gravity, m/sec^2
Kn	=	Knudsen number
m	=	mass, kg
Δp	=	pressure differential, Pa
q_∞	=	free stream dynamic pressure, Pa
R	=	specific gas constant
R_n	=	nose radius of entry vehicle, m
R_t	=	radius of ballute minor torus, m
R_t'	=	distance from centerline of ballute to minor torus center, m
s	=	molecular speed ratio
T_∞	=	ambient atmospheric temperature, K
V_∞	=	vehicle velocity, m/sec
β_b	=	ballute ballistic coefficient,
θ	=	inclination angle, deg
θ_b	=	ballute half cone angle, deg
γ	=	flight path angle, deg
ϕ_{tank}	=	tank mass factor, m
σ_n	=	normal accommodation coefficient
σ_t	=	tangential accommodation coefficient

* Graduate Research Assistant, Guggenheim School of Aerospace Engineering, Student member AIAA.
† Associate Professor, Guggenheim School of Aerospace Engineering, Associate Fellow AIAA.

I. Introduction

THE problem of Earth return from the Moon can be summarized as the requirement to dissipate the large amount of kinetic energy associated with an entry vehicle on a lunar return trajectory. Common approaches to this problem are to use the aerodynamics of the entry vehicle to decelerate in a controlled process and/or to tailor the entry trajectory so as to dissipate energy in a benign manner. For the former approach, direct application of drag requires the entry vehicle to reach an appreciable level of atmospheric density, which increases the heat rate and magnitude of deceleration felt by the vehicle. Whereas deceleration at higher altitudes and lower densities is preferable, constraints on vehicle shape and size may not allow for the large drag coefficients and reference areas required. However, reference area can be drastically altered through the use of an inflatable drag device commonly termed a ballute. Through an increase in reference area, a ballute provides several advantages during planetary entry and descent. By achieving improved deceleration at lower atmospheric densities the heating rates encountered can be significantly lessened. A large ballute also serves to increase the effective nose radius of the entry vehicle, providing further reduction in the convective heat rate, though with the potential of increasing of the radiative heat rate. Additionally, a ballute can expand an available entry corridor by preventing skip out at shallower flight path angles. These benefits have the potential to improve the mass fraction devoted to a vehicle's entry system by reducing the required heat shield mass and improving the payload volume fraction. Ballute technology may also provide a reasonable alternative for cases where thermal protection systems are not yet qualified or where complete elimination of TPS failure modes is desired.

First theorized in the early 1960's, ballutes (from the contraction of balloon and parachute) have long been envisioned for a variety of mission concepts including aerocapture at Mars[1] or Saturn's moon Titan[2]. More recently, emphasis has been placed on maturing the designs and technologies associated with deployable systems. Towards this end, flight demonstrations such as the IRDT-1 mission[3] and the upcoming Inflatable Reentry Vehicle Experiment (IRVE) mission[4] have sought to characterize the behavior of ballutes under reentry conditions. For a more extensive history, the reader is directed to the survey paper by Rohrschneider and Braun[5].

Entering the Earth's atmosphere from a lunar return trajectory is one of the more difficult tasks facing future human exploration. With entry velocities roughly 40% higher than a typical entry from low Earth orbit, limitations on a vehicle's heating and deceleration can quickly be overwhelmed. During the Apollo program, reentry of the Command Module at 11 km/sec resulted in peak heat rates between 250 and 300 W/cm^2 and a peak deceleration of over seven g's[6]. A return trip to the moon using a vehicle larger and heavier than the Apollo Command Module, as is currently envisioned, will encounter more severe conditions upon Earth reentry. The Crew Exploration Vehicle is being designed to tolerate a peak heat rate on the order of 1000 W/cm^2. The high heating rates encountered by the Apollo Command Module dictated the use of an ablative thermal protection system (TPS). Although ablative systems are frequently used in robotic exploration missions, the production line for the original ablative material used by the Apollo program, AVCOAT, was shut down for several decades[7] and thus a new material will either need to be developed or an existing material re-certified for use on human exploration missions. Given that both of these options represent potential risk and significant investment, an alternative technology path consisting of ballute-based entry may merit parallel investigation. Such a system has the potential to mitigate heating rates sufficiently, reducing the performance requirements of the ablative TPS and the mass of such a system, or allow for the use of an already developed reusable TPS concept. While mitigating or eliminating TPS failure modes, a ballute system is not without its own development complexity and risk.

The focus of this paper is to assess the feasibility of using a ballute for a human exploration vehicle returning on a lunar trajectory. This is done by first quantifying the impacts that a ballute can have on a lunar return entry trajectory with regards to heating and deceleration and then subsequently sizing the ballute entry system. This study also explores different deployment strategies for using a ballute, including an early jettison of the ballute after a predefined velocity decrement. Trends are explored that can assist in determining the performance metrics of a ballute entry system. As the impetus for this study is the Vision for Space Exploration, emphasis is placed on the impacts that a ballute entry system has on the baseline Crew Exploration Vehicle.

II. Approach

The study was broken into two phases with the first seeking to quantify the advantages ballutes can offer during entry and the second seeking to investigate sizing trends of ballutes. The first phase consisted of running a broad range of entry trajectories over a variety of ballute sizes and quantifying the magnitude and profile of deceleration, the heat rate profile, and the dynamic pressure experienced by both the ballute and the CEV. This was done across multiple entry strategies. The initial strategy consisted of utilizing the ballute from atmospheric entry through a subsonic velocity. An alternative strategy investigated is a hybrid direct-entry approach where the ballute is used to

impart a sufficient velocity decrement to make the remainder of the entry aerothermodynamically-equivalent to entry from low earth orbit. That is, the ballute is used to decelerate the CEV to LEO velocities (~7.8 km/sec) and is subsequently jettisoned. The potential advantages of this approach include reducing the heating and pressure loads on the ballute while mitigating the heating and deceleration profiles seen by the CEV to those consistent with initial plans for the CEV (LEO entry). Within this approach, two separate post-jettison entries were investigated, an operationally-simple ballistic entry and a low-L/D lifting entry. Although the study primarily focused on a crewed entry vehicle, investigations into a lower mass cargo variant of the CEV were also performed.

To assist in evaluating a large number of configurations, entry trajectories, and deployment strategies, analysis methods suitable for a conceptual design were used. The linkage between disciplines in this study is visualized in the design structure matrix (DSM) shown in Figure 1. Each of the connections between the disciplines represents the flow of information between the contributing analyses. As per the scope of the study, the results attained focus on examining the feasibility of a ballute system from a conceptual level and do not seek to offer quantitative validation that the concepts explored are feasible in regards to higher level analyses, e.g. aeroelastic and structural dynamic response.

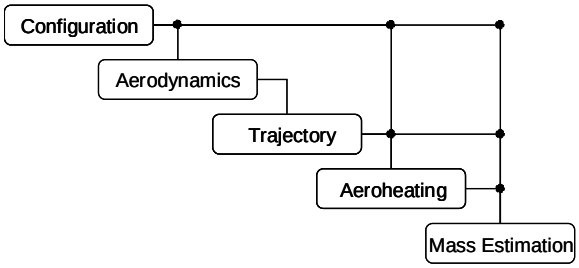

Figure 1. DSM for ballute analysis.

A. Configuration

An entry vehicle configuration was selected consistent with the CEV design chosen by NASA's Exploration Systems Architecture Study[8]. In particular, the vehicle's shape is based on the Apollo Command Module with a 5.5 meter base diameter. Other major dimensions are outlined in Figure 2. The nose radius was linearly scaled as well from an Apollo value of 4.6 meters to a new value of 6.4 meters. Lastly, the mass of the crewed entry vehicle was kept fixed at 9500 kg, the ESAS-estimated mass of the lunar variant of the CEV. Subsequent analyses examining a cargo variant of the CEV kept the vehicle dimensions the same, but varied the entry mass from 2000 kg to 9000 kg.

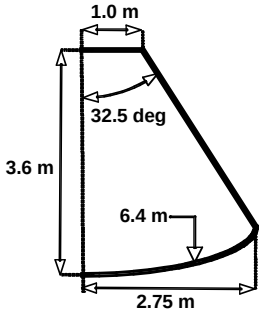

Figure 2. Entry vehicle shape and dimensions.

Though many ballute mission profiles have been previously studied, a majority focus on three distinct ballute configurations, shown in Figure 3. The trailing torus design consists of an inflated ring that is attached to the entry vehicle by a series of tethers. The trailing sphere is of a similar nature, though replaces the torus shape with a simple sphere. The clamped torus does away with tethers and instead attaches the torus to the entry vehicle with a conical frustum that fully encloses the CEV.

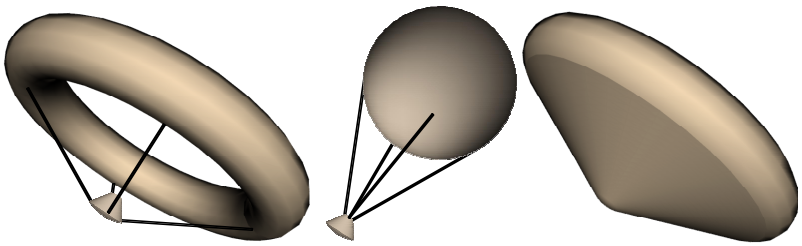

Figure 3. Trailing torus, sphere, and clamped torus ballutes.

A ballute's capacity to decelerate the entry vehicle can be measured by its drag area. The drag produced by the ballute must in turn be balanced by the relative mass contribution of the ballute. That is, a large trailing sphere may produce as much drag as a medium sized clamped torus; however the trailing sphere may require less material and pressurant and therefore be less massive. Assuming that the majority of a ballute system's mass comes from the ballute material then a simple way to compare ballute types is through use of a ballute ballistic coefficient, β_b. Conventionally, the ballistic coefficient is calculated as the ratio of a vehicle's mass to its drag contribution. An alternative representation that is useful in comparing ballute characteristics is to simply use the ballute's surface area rather than its mass. Under these rules, the ballute ballistic coefficient can be defined as follows.

$$\beta_b = \frac{Ballute\ Surface\ Area}{C_D A_{ref}} \tag{1}$$

Using this dimensionless form of the ballistic coefficient, if two ballutes have the same surface area, and thus roughly the same mass, the one with the lower value of the ballute ballistic coefficient would produce a greater degree of drag and deceleration. Thus, a lower value of β_b is typically favored as it represents a more effective ballute. The respective values of β_b for the three ballute types are summarized in Table 1. The notation used for defining the trailing and clamped torus ballutes is outlined in Figure 4. Note that in the calculation of C_D and β_b, the reference area, A_{ref}, is computed based upon the entire diameter of the ballute, not just an exposed area. The hypersonic drag coefficients listed in Table 1 are calculated from Newtonian aerodynamics. From these calculations it can be seen that the advantage the trailing torus provides in reduced surface area versus the clamped version is insufficient to overcome its significantly lower drag contribution. Of the three ballute types the trailing sphere is calculated as having the lowest β_b.

Table 1. Ballute performance characteristics for a torus ratio (R_t'/R_t) of five and CEV dimensions.

Ballute Type	Surface Area (m^2)	Hypersonic C_d	β_b
Trailing Torus	$\pi^2 D_b^2 \frac{R_t'/R_t}{\left(R_t'/R_t+1\right)^2}$	0.741	7.9
Trailing Sphere	πD_b^2	1.0	4.0
Clamped Torus	$\pi^2 D_b^2 \frac{R_t'/R_t}{\left(R_t'/R_t+1\right)^2} + \frac{\pi\left(D_b^2 - D_c^2\right)}{2\sin\theta_b}$	1.496	5.9

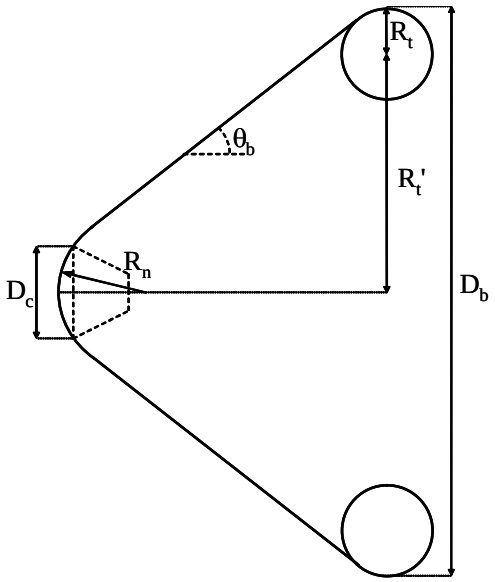

Figure 4. Toroidal ballute geometry definitions.

Though ballutes are often considered solely for their drag characteristics, the clamped configuration offers advantages in the heating regime as well. Because of the separation distance of the towed ballute from its entry vehicle the ballute can be exposed to adverse wake effects coming off the entry vehicle. Previous studies focusing on these effects[9,10] noted several vehicle/ballute behaviors including the possibility of unfavorable flow choking in the core of a trailing torus and increased heating to the base of the vehicle due to reverse flow. In the case of the trailing sphere, impingement of the entry vehicle shock on the ballute produced levels of localized heating that were as high as twice those seen by the sphere alone. Heating results on the clamped ballute were the most favorable. Since the clamped ballute is attached directly to the base of the entry vehicle the boundary layer fully envelops both the ballute and the spacecraft. This has the effect of greatly increasing the effective nose radius of the entry vehicle thereby reducing convective heating significantly. Given that convective heating to the delicate ballute is more likely to be a limiting factor than heating to the entry vehicle, a further advantage of the clamped configuration is that the ballute and entry vehicle are exposed to roughly the same heat rates. Lastly, although a clamped ballute would be 2-3 times more massive than a trailing ballute of an equivalent diameter, the reduction in heat rate provided by the clamped ballute allows for an overall smaller diameter and thus reduced system mass.

In summary, although the trailing sphere is favorable for its approximate mass to drag contribution ratio, the heating advantages provided by the clamped configuration are more applicable to the mission scenario being studied. In view of this, the analysis henceforth will focus on using a clamped torus ballute.

B. Aerodynamics

As mentioned previously, the entry vehicle analyzed was a scaled up version of the Apollo Command Module. Because of the extensive amount of testing already done on this shape, aerodynamic data is readily available. Thus, the aerodynamic properties used for the entry vehicle were taken from published data[11].

For many of the ballute diameters evaluated, a sizeable portion of the entry trajectory is characterized with Knudsen numbers on the order of unity. Even though this does not place the ballute fully in the free-molecular flow regime (often estimated as Kn $\geq$ 10) it does indicate that transitional regime aerodynamics are important. To attain transitional values, the free-molecular and continuum aerodynamics were first estimated and then a bridging function was utilized. The free-molecular drag coefficients were calculated assuming a diffuse Maxwellian reflection model[12] where the values of the normal and tangential momentum accommodation coefficients, σ_n and σ_t respectively, are assumed equal to one. Calculation of the free-molecular pressure and shear forces was done using the following relations[12]:

$$\begin{aligned}\frac{\Delta p}{q_\infty}s^2 = &\left[\frac{(2-\sigma_N)}{\sqrt{\pi}}s\sin\theta + \frac{\sigma_N}{2}\left(\frac{T_w}{T_\infty}\right)^{1/2}\right]\exp\left(-s^2\sin^2\theta\right)\\ &+\left[(2-\sigma_N)\left(1/2+s^2\sin^2\theta\right)+\frac{\sigma_N}{2}\left(\frac{T_w}{T_\infty}\right)^{1/2}\sqrt{\pi}s\sin\theta\right]\left[1+\operatorname{erf}\left(s\sin\theta\right)\right]\end{aligned} \tag{2}$$

$$\frac{\Delta\tau}{q_\infty}s^2 = \frac{\sigma_N s\cos\theta}{\sqrt{\pi}}\left\{\exp\left(-s^2\sin^2\theta\right)+\sqrt{\pi}s\sin\theta\left[1+\operatorname{erf}\left(s\sin\theta\right)\right]\right\} \tag{3}$$

The molecular speed ratio, *s*, is comparable to the Mach number and can be calculated as follows:

$$s_\infty = \frac{V_\infty}{\sqrt{2RT_\infty}} \tag{4}$$

Since the ballute shape is a relatively simple one it is possible to numerically integrate the above relations over the surface of the ballute to attain values for the aerodynamic coefficients.

In the continuum regime drag coefficients were estimated from Newtonian impact theory. Under this method the tangential or shear forces are neglected and a simple relation for the pressure coefficient on an elemental area inclined to the freestream at an angle θ can be derived as:

$$C_p \equiv \frac{\Delta p}{q_\infty} = 2\sin^2\theta \tag{5}$$

As opposed to the free-molecular pressure and shear coefficients, the Newtonian relation allows for an explicit integration over the surface of ballute. As such, the zero angle of attack drag coefficient for a clamped torus ballute can be calculated from the following:

$$\begin{aligned}C_{D,ballute} = &\left(\frac{R_n}{R_b}\right)^2\left[1-\sin^4\theta_b\right]+2\sin^2\theta_b\left[\frac{\left(R_t'+R_t\cos\theta_b\right)^2}{R_b^2}-\left(\frac{R_n}{R_b}\right)^2\cos^2\theta_b\right]\\ &+\frac{4R_t\left(R_b-R_t\right)}{3R_b^2}\left[2-3\cos\theta_b+\cos^3\theta_b\right]+\left(\frac{R_t}{R_b}\right)^2\sin^4\theta_b\end{aligned} \tag{6}$$

The reference area used to non-dimensionalize the above relation is based upon the ballute radius, R_b. Additionally, Eq. (6) can be broken down by the contribution of each of the three main geometric elements of the clamped torus

ballute. The first term in Eq. (6) is the drag coefficient of the spherical nose portion, the second term is the drag of the conical frustum, and the last terms comprise the drag from the exposed portion of the torus itself. For a given set of entry vehicle dimensions the ballute half cone angle, θ_b, can be calculated by assuming a smooth interface between the ballute and the entry vehicle heat shield yielding the following:

$$\theta_b = \cos^{-1}\left(\frac{D_c}{2R_n}\right) \tag{7}$$

Using the entry vehicle dimensions mentioned previously a ballute cone angle of roughly 65 degrees is calculated and is used for this study.

Determination of the transitional regime drag coefficients was done using the bridging function of Gorenbukh[12] provided below.

$$\frac{C_D - C_{D,cont}}{C_{D,FM} - C_{D,cont}} = \frac{1}{\sqrt{2\pi}} \int_{-\infty}^{\log_{10}(Kn)+1.1403} \exp\left(-y^2/2\right) dy \tag{8}$$

C. Trajectory

The analysis of atmospheric entry at Earth was done using the three-degree-of-freedom version of the Program to Optimize Simulated Trajectories (POST)[13] assuming a standard 1976 atmosphere. Entry velocities were kept constant at an inertial value of 11.1 km/sec. Atmospheric interface was assumed to occur at an altitude of 125 km. Entry flight path angles were varied to within 1/20th of a degree over a five degree corridor so as to closely evaluate skip-out boundaries for each diameter. This level of resolution was needed because many of the more favorable ballute entry trajectories are those that are near the limits of skip-out, spending a significant amount of time in the upper atmosphere.

For this study, multiple entry trajectory strategies were investigated. In all cases, the ballute was assumed deployed in-space prior to reaching atmospheric interface. The first strategy consisted of using the ballute through the entire entry. An alternative strategy is to simply jettison the ballute after some predetermined velocity decrement has occurred. This concept represents a hybrid aerocapture/direct entry approach that attempts to use the ballute to dissipate energy until the lunar entry becomes similar to entry from low Earth orbit. In this strategy, the trajectory segment that made use of the ballute was flown with a zero angle-of-attack. Subsequent to ballute jettison, ballistic and lifting (L/D=0.3) CEV trajectory options were investigated. An L/D of 0.3 is based upon that provided by the Apollo capsule at its trimmed angle of attack.

D. Aeroheating

Estimations of the aeroheating encountered by the ballute and entry vehicle were done using two stagnation point heating approximation methods. Convective heating was calculated using the correlation provided by Sutton and Graves[14]. During Earth entry at lunar return velocities, radiative heating from the shock layer contributes considerably and must be accounted for. Towards this end, the method for estimating radiative heat rates by Tauber and Sutton[15] is used. A major variable in both formulations is the effective nose radii. For large clamped ballutes this nose radius is much greater than that of the entry vehicle alone. Examination of CFD cases completed as part of the aerocapture technology portion of NASA's In Space Propulsion program[16] indicated that the effective nose radius of a clamped ballute as a percentage of the ballute diameter increases as the ballute diameter increases. For this study an approximation was used that estimated the effective nose radius to be a quarter of the diameter for a 25 m ballute and three quarters the diameter of any ballute larger than 100 m. Although larger effective nose radii significantly reduce convective heating, they also lead to increased radiative heating since convective heat rates are proportional to the inverse square root of the nose radius while radiative heat rates are roughly proportional to the nose radius itself[17]. Thus, depending on the proportion of peak heating due to radiative effects, larger ballute diameters can actually incur higher heating rates than smaller ones. Though this general behavior is captured by the two heating methods employed, more detailed analysis will be required to validate the calculated levels of heating, particularly by the radiative portion.

E. Mass Estimation

The total ballute entry system was considered as four components consisting of the ballute material, the pressurant required to inflate the ballute, the pressurant tankage, and a fixed mass associated with pressure transducers, valves, fittings, and other mechanical/electrical systems. Ballute mass was calculated from the total surface area of the ballute for a given average areal density of ballute material. Pressurant mass was calculated as a function of the internal volume of the ballute using nitrogen gas. The amount of nitrogen required was determined by assuming a required ballute inflation pressure of twice the peak dynamic pressure with a 15% margin. With the amount of required nitrogen known, tankage mass was estimated using the following simple relationship[18]:

$$m_{\text{tank}} = \frac{m_{N_2} R_{N_2} T_{\text{tank}}}{g_0 \phi_{\text{tank}}} \tag{9}$$

For the tank-mass factor, ϕ_{tank}, a value of 6350 m corresponding to a typical titanium pressurant tank was used.

III. Results and Discussion

A. Trajectory and deployment impacts

The first portion of this investigation focused on evaluating the trajectory and heating characteristics of a ballute entry for a 9500 kg CEV. This goal included both a characterization of the entry design space and an examination of multiple ballute entry strategies. CEV assumptions, entry mass, and ballute half-cone angle were kept constant and the ballute diameter was varied (from 30 to 200 m). A clamped torus ballute configuration was assumed. Atmospheric interface conditions for each of the trajectories consisted of an 11.1 km/sec inertial velocity over a range of inertial flight path angles. This entry velocity corresponds to an approximate three-day transit from lunar orbit and is the entry velocity attained by the Apollo missions.

For entries that retain the ballute to the surface, the primary metrics of interest were peak heating, deceleration, and dynamic pressure. The first of these is provided in Figure 5 along with a shaded region corresponding to overshoot conditions. The overshoot boundary is defined as the point at which the vehicle will no longer reach the surface and will either continue on an escape trajectory or enter Earth orbit. At lower ballute diameters, modest increases in ballute diameter exhibit large decreases in peak heating due to both deceleration at higher altitudes and to an increased effective nose radius. However, this trend quickly plateaus as the proportional change in ballistic coefficient becomes less and the effective nose radius increases to 75% of the ballute diameter. Although material heating limits are discussed in greater detail in a subsequent section, candidate materials (without the addition of TPS) typically have temperature limits less than 1000 K, which corresponds to heating limit of roughly 4.5 W/cm^2. Under those constraints ballute diameters of at least 110 meters will be required for Earth entry.

The second metric of interest is primarily due to the inclusion of human passengers on this lunar return vehicle. As shown in Figure 6, for a given flight path angle, the peak deceleration tends to decrease with decreasing ballute

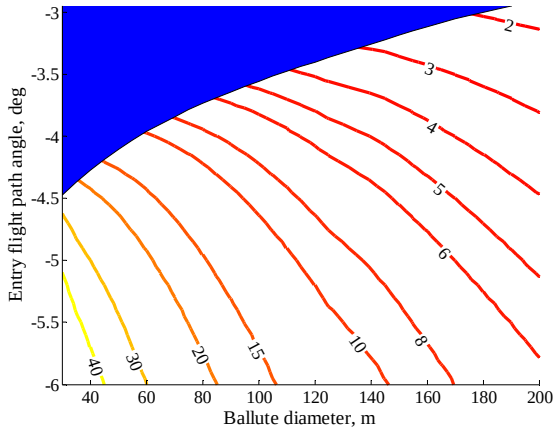

Figure 5. Peak heat rate (W/cm^2) contours for an 11.1 km/sec, 9.5 MT entry without ballute jettison.

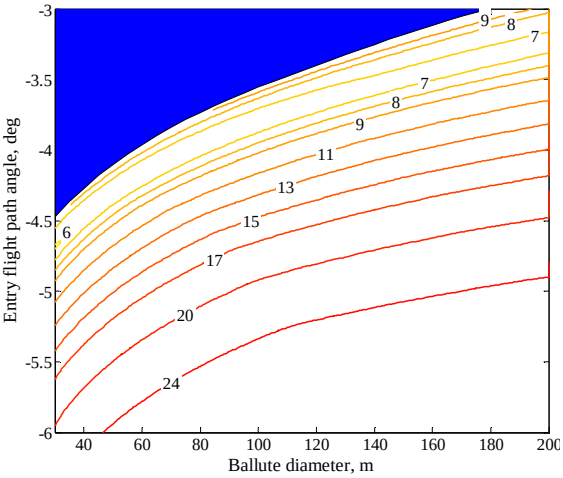

Figure 6. Peak deceleration (g's) contours for an 11.1 km/sec, 9.5 MT entry without ballute jettison.

size. More interesting perhaps is that unlike peak heat rate, for a fixed ballute size the minimum value of peak deceleration does not occur at the overshoot condition but rather a few tenths of a degree away from this boundary. This indicates that entry trajectories that seek to minimize peak heat rate do so at the expense of increased deceleration loads. In the case of the 4.5 W/cm^2 heating constraint, this would either mean keeping the 110 meter ballute and taking the penalty in g-loads (approximately 9 g's) or moving to a larger ballute so as to be able to tolerate the increased heat rate of a slightly steeper entry. This also gives insight into the width of the deceleration limited entry corridors. For example, restricting an entry to 7 g's, the same as that encountered by the Apollo astronauts, implies a total corridor width of about a quarter of a degree (well within demonstrated navigation capabilities).

Results for peak dynamic pressure are provided in Figure 7. Occurring simultaneously with peak deceleration, peak dynamic pressure is of interest primarily for its impact on the design of the ballute. In particular, a lower peak dynamic pressure allows for lower inflation pressures, reduces material strength requirements, and reducing the likelihood of adverse structural dynamic response. Again limiting the ballute to a heat rate of 4.5 W/cm^2 it can be seen that dynamic pressures of no more than 75 Pa and closer to 50 Pa will be encountered. As was the case with the deceleration contours, the optimum dynamic pressure conditions do not occur at the overshoot boundary.

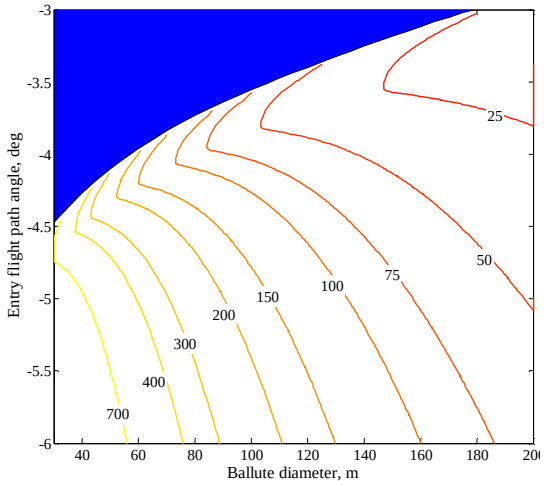

Figure 7. Peak dynamic pressure (Pa) contours for an 11.1 km/sec, 9.5 MT entry without ballute jettison.

Altitude, velocity, and deceleration profiles are provided in Figure 8 for a 100-m diameter ballute system over a range of entry flight–path angles. Entry at flight path angles just shy of the overshoot boundary results in multiple skips. During the first portion of the entry the ballute is able to dissipate enough energy so as to remain on an eventual touchdown trajectory though not without first exiting the atmosphere. The deceleration profile is thus multi-pulsed with the majority of the deceleration occurring during the second entry. As the entry flight path angle steepens, more deceleration is performed early on and the magnitude of the second pulse lessens. The minimal peak deceleration occurs when the two pulses are roughly equivalent (γ = -3.8° with a peak deceleration of approximately 5 g's for the example in Figure 8). This comes at the expense of an extended pulse duration. Further steepening of the entry merges the two pulses and the maximum deceleration value begins to increase again.

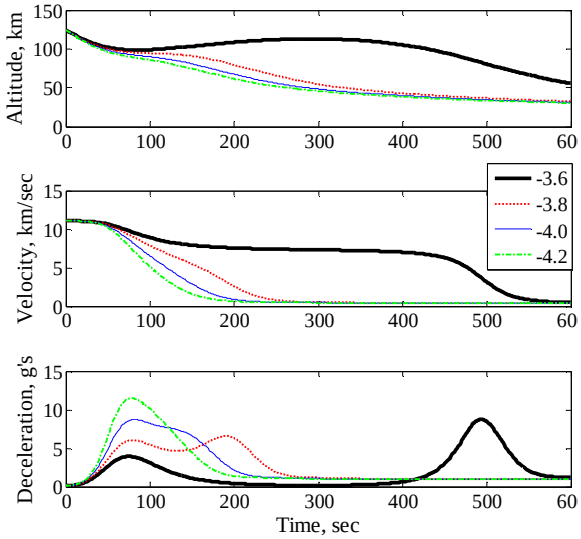

Figure 8. Altitude, velocity, and sensed deceleration profiles for a 100 meter diameter ballute over a range of entry flight path angles.

For a 9500 kg CEV payload, the entry strategy of not jettisoning the ballute is shown to require a ballute diameter greater than 100 m, depending on the heating and dynamic pressure limits placed on the ballute. It should be mentioned that although this entry strategy is referred to as not jettisoning the ballute, this is in reference to hypersonic flight. Because of safety and heritage concerns, descent and landing across supersonic and subsonic conditions would most likely be performed under the canopy of a parachute. Although previously proposed for landing large payloads on Mars[19], retention of the ballute through transonic and subsonic conditions would require significantly more knowledge in the behavior of inflatable structures than is encompassed in this study.

An alternative to retaining the ballute through most of the entry is to deploy the ballute for only a predetermined duration or velocity decrement and then release the ballute. In a typical aerocapture strategy the ballute is used to

dissipate enough energy from the hyperbolic approach trajectory to transition to a closed Earth orbit in a single pass. In this investigation, a hybrid entry strategy is proposed that enters at a slightly steeper angle so that upon ballute release the entry vehicle follows a second Earth entry trajectory. In this manner, the loads encountered by the ballute are traded against those placed on the CEV. Releasing the ballute earlier tends to increase the heating encountered by the CEV but also mitigates the strength and thermal requirements of the ballute. Further demonstration of this effect is provided in Figure 9 where different release velocities are plotted against a no-release trajectory for a 100 m diameter ballute entering at a -3.6 degree inertial flight path angle. For this trajectory, ballute jettison occurs prior to the second, stronger dynamic pressure pulse, reducing the peak dynamic pressure encountered by the ballute. Attempting to further lessen the dynamic pressure proves impossible as the initial pulse occurs well before the ballute has provided enough velocity change to allow for an Earth entry. For the same reasons, heating limitations on the ballute can not be avoided as peak heating occurs at velocities of about 10.5 km/sec.

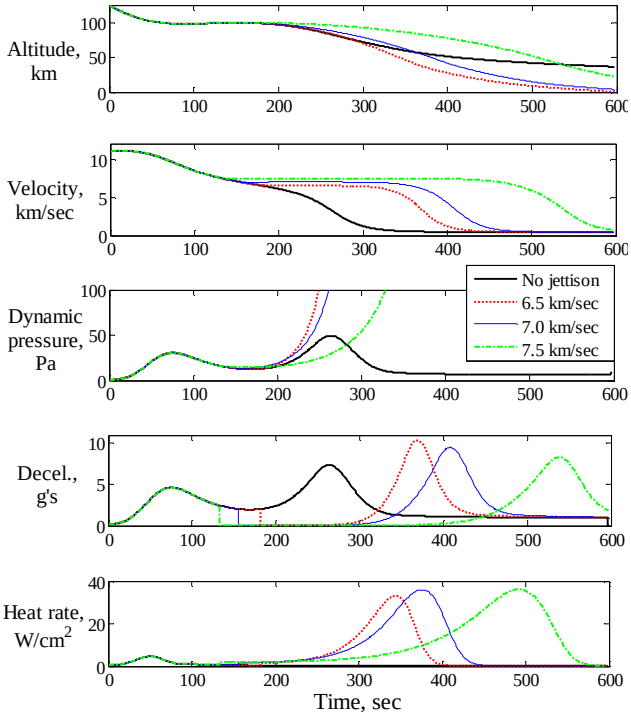

Figure 9. Trajectory effects of varying jettison velocities on a near skip-out entry of a 9.5 MT vehicle using a 100 m ballute and entering at 11.1 km/sec (post jettison entry is at a zero angle of attack).

Descent after ballute jettison was evaluated under two separate conditions, one where the vehicle continued on a ballistic, zero angle-of-attack trajectory and the other where the vehicle transitioned to a low-L/D lifting trajectory with an L/D of 0.3. The former approach is favorable for its simplicity while the latter approach may be necessary for targeting purposes. Beginning with the ballistic condition, entries with ballute jettison can be shown to provide several advantages. Shown in Figure 10 are entry vehicle heating contours over a range of inertial jettison velocities. Provided on the abscissa are the peak heating rates on the ballute prior to jettison. Examination of the heating rates encountered by the entry vehicle after ballute jettison shows the potential to mitigate peak heat rates to less than 35 W/cm^2, or roughly the limit of an existing reusable thermal protection system. Also evident is that this capability exists over a range of ballute diameters with the primary constraint being the heating limitations on the ballute itself. These lower heating rates can be attained at two separate ranges of jettison velocities, a higher range that lets the entry vehicle alone decelerate more at higher

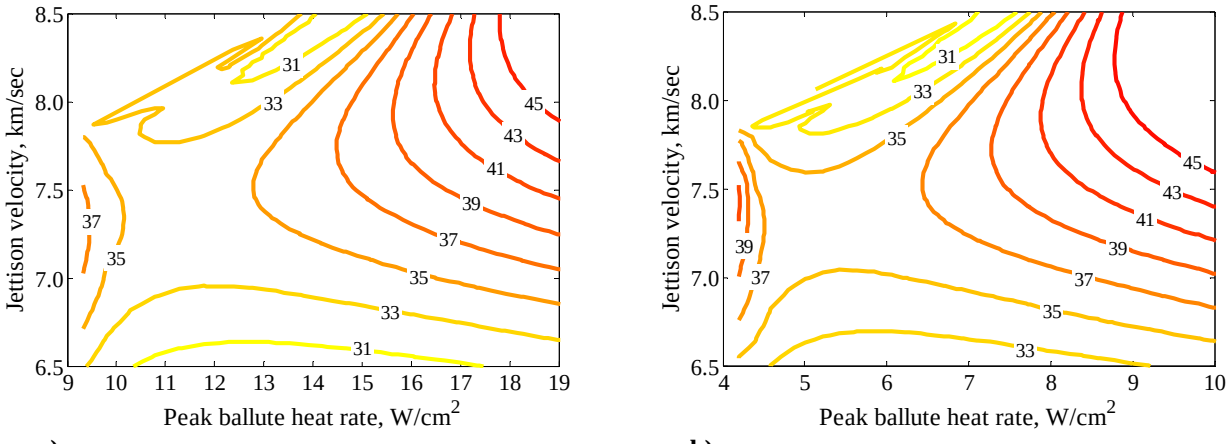

Figure 10. Peak entry vehicle heat rate (W/cm^2) contours with zero angle of attack entry after jettison for ballute diameters of a) 65 m and b) 110 m.

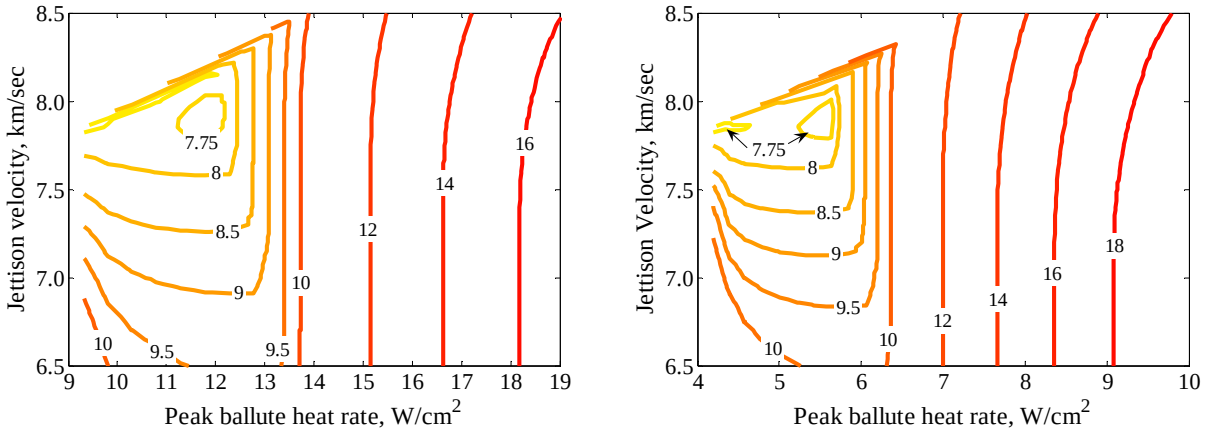

a.) **b.)**

Figure 11. Peak deceleration contours (g's) for zero angle of attack entry after jettison of a) 65 m and b) 110 m ballutes.

altitudes and a lower range that releases the entry vehicle in a thicker atmosphere but also at a lower speed. Provided in Figure 11 are peak deceleration contours over a range of jettison velocities. The peak deceleration values plotted correspond to the larger value of either the peak deceleration with the ballute or the peak deceleration seen after ballute release. At the lower ballute heat rates (shallower entry angles), peak deceleration occurs after ballute jettison. At steeper entry angles the ballute deceleration pulses are merged and peak g's are seen prior to ballute release. Although favorable heating conditions can occur at both low and high jettison velocities, deceleration considerations are shown to favor high jettison velocities as they eliminate the second, larger ballute deceleration pulse. Figure 12 shows the peak dynamic pressures the ballute is exposed to prior to ballute jettison. In contrast to retaining the ballute, jettison can reduce the maximum dynamic pressures by as much as 50%, particularly for entry conditions near skip-out where the stronger pressure pulse is avoided. Whereas previously achieving the lowest dynamic pressures meant entering at steeper angles and thus incurring higher heat rates, ballute jettison is able to collocate minimum heating and minimum dynamic pressure at the overshoot boundary. Though not shown, variation of the velocity at which the ballute was released had little or no impact on the peak dynamic pressures.

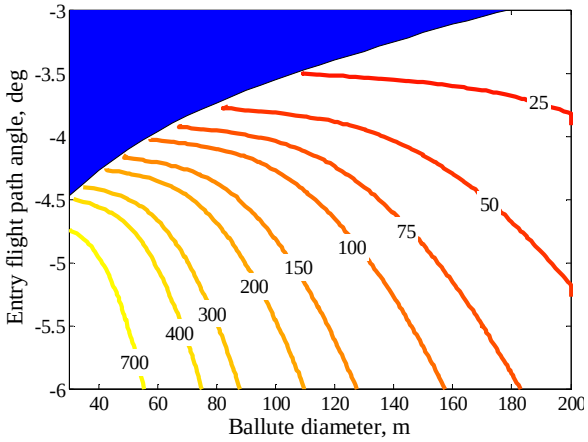

Figure 12. Peak dynamic pressures (Pa) encountered by ballute prior to jettison for a 9.5 MT, 11.1 km/sec entry.

Entry vehicle heating contours for a lifting post-ballute entry are shown in Figure 13. Peak entry vehicle heat rate (W/cm2) contours with lifting entry after jettison for ballute diameters of a) 65 m and b) 110 m.. Compared to the ballistic entry, using a moderate degree of lift reduces the entry vehicle heat rates to well within reusable limits for nearly all of the entry angles and jettison velocities evaluated. Again, this trend holds over a range of ballute diameters, once more indicating that the thermal limitations of the ballute material (as indicated by the abscissa in Figure 10 and Figure 11) will drive the required ballute size more than the requirement for a certain amount of velocity change. That is to say, small ballutes can be used to significantly reduce CEV heating just as well as large ballutes, so long as the ballutes themselves are capable of handling the increased heating. Improvements in peak g's, shown in Figure 14, are also evident when lift is introduced. At the shallowest entries, maximum deceleration can be reduced to 4-4.5 g's, depending on the ballute size. Additionally, the peak deceleration is shown to be almost completely independent of the jettison velocity.

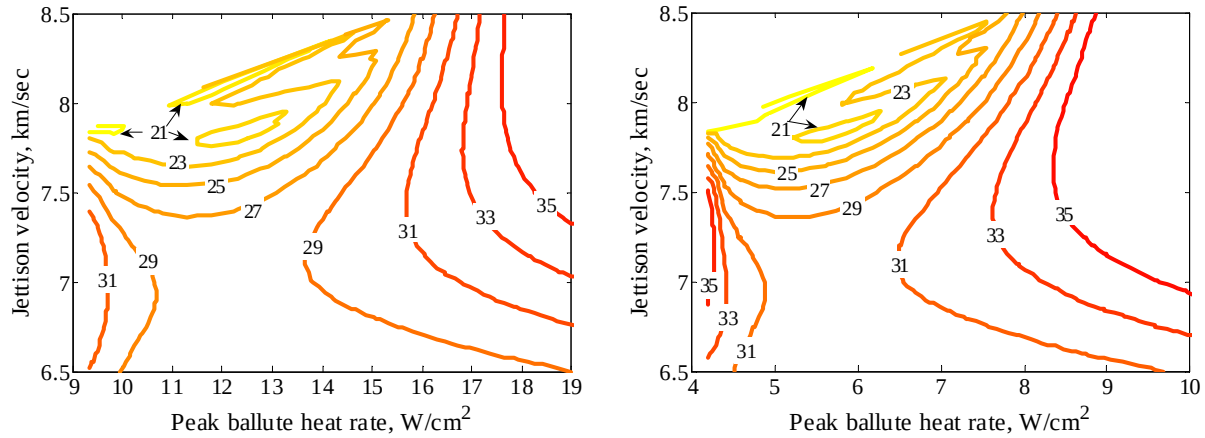

Figure 13. Peak entry vehicle heat rate (W/cm^2) contours with lifting entry after jettison for ballute diameters of a) 65 m and b) 110 m.

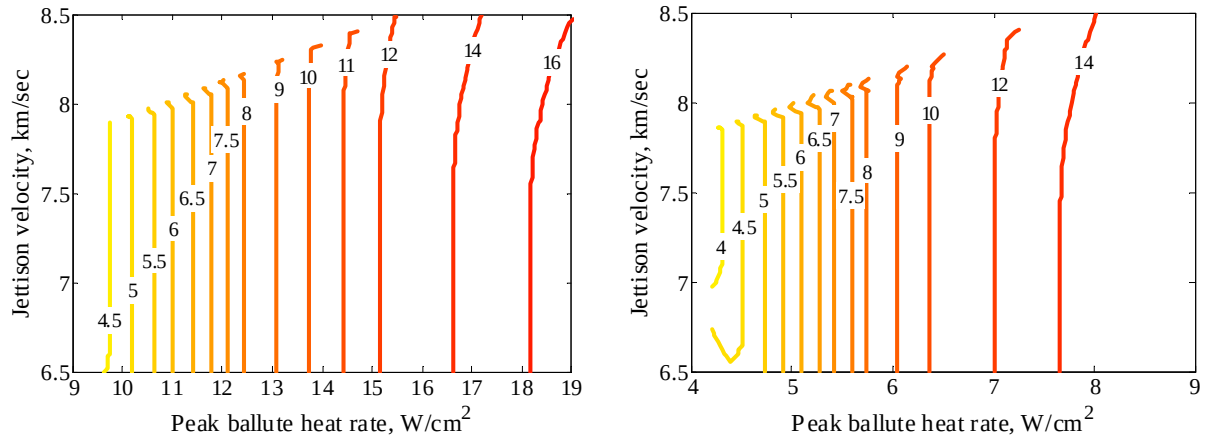

Figure 14. Peak deceleration contours (g's) with lifting entry after jettison for ballute diameters of a) 65 m and b) 110 m.

In addition to the 9500 kg crewed CEV, investigations into lower mass cargo vehicles using the same basic dimensions as the CEV were performed. As it is not expected that cargo variants will have as strict a requirement on deceleration loads as a crewed vehicle, only ballute entries that retain the ballute were investigated. The primary metrics of interest were heat rates, dynamic pressures, and overshoot boundaries, shown in Figures 15-17.

Minimum heat rate results for this portion of the study are provided in Figure 15. These heat rates correspond to entry at flight path angles equivalent to the overshoot boundary and thus correspond to the minimum heat rate possible for a given entry mass and ballute size. Again using a 4.5 W/cm^2 heat rate limitation, it can be seen that each reduction in entry mass of a 1000 kg allows for a roughly 10 m reduction

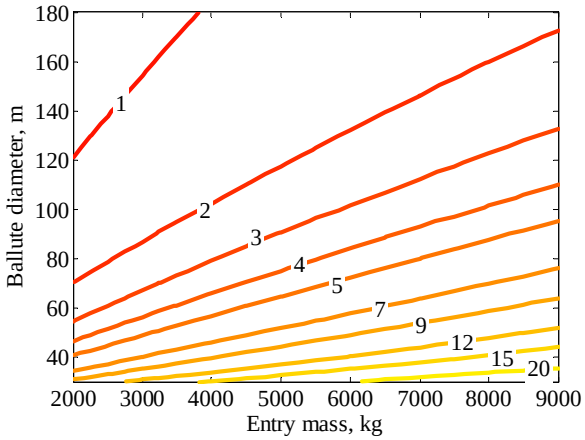

Figure 15. Peak heating (W/cm^2) contours at the overshoot boundary of an 11.1 km/sec.

in required ballute diameter. This 100:1 ratio provides an excellent rule of thumb for future lunar entry design considerations.

Contours of peak dynamic pressure and overshoot boundaries are provided in Figure 16 and Figure 17 respectively. The plotted dynamic pressure values correspond to entry flight path angles yielding the lowest peak dynamic pressure and do not necessarily correspond to the overshoot boundaries.

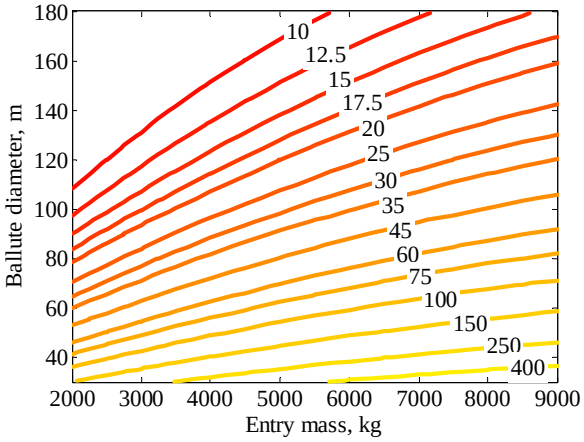

Figure 16. Minimum peak dynamic pressures (Pa) for an 11.1 km/sec entry over a range of entry masses and ballute diameters.

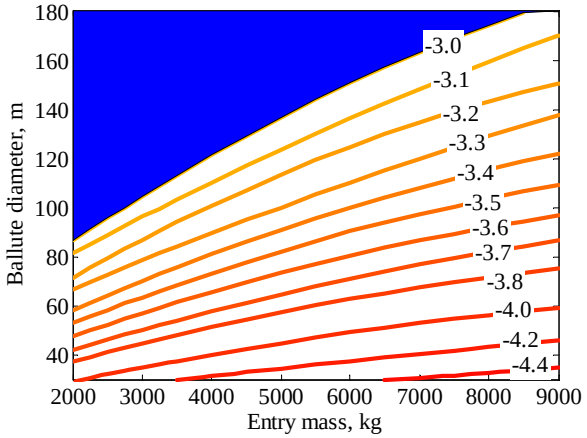

Figure 17. Overshoot boundaries for an 11.1 km/sec entry over a range of entry masses and ballute diameters.

B. Sizing and Mass Evaluation

The second portion of the study focused on evaluating the mass of a candidate ballute entry system. From the simple mass model introduced earlier several sizing trends can quickly be observed. Provided in Figure 18 are contours of ballute systems masses for different size ballutes and material densities. At larger diameters, attaining a ballute system mass on the order of several metric tons requires an average material density of 0.15 kg/m^2 or less. Note that the slope of the contours provides insight into the relative importance of the material areal density on the total system mass. In particular, for a constant ballute diameter, doubling the areal density nearly doubles the ballute system mass. Indeed, for a fill pressure of 100 Pa the mass of the ballute material alone represents almost 85% of the total ballute system mass at even the lowest areal densities. Though not shown, doubling or halving the fill pressure changes the relative contribution to about 75% and 90% respectively.

Given its importance in determining the overall mass of a ballute system, achieving a low material weight is a primary technical hurdle towards a feasible ballute system. Achieving low areal densities is complicated by the thermal and strength limitations of many candidate materials. Previous conceptual studies[1,20] have focused on using thin-film materials such as Kapton and Polyboxoxazole (PBO) which have operational temperature limits of around 500 °C and areal densities of about 0.075 kg/m^2. The low temperature limits of thin-films have led to a focus on using various types of multi-layer insulation (MLI). These concepts typically consist of one of the above polymer films as an internal bladder combined with additional layers of adhesives, metal foils, and outer layer fabrics such as Nextel that are designed to resist much higher heating conditions. One such concept[21] was evaluated at heating rates as high as 35 W/cm^2 without observable damage. Although this concept had a sizeable average areal density of about 1.86 kg/m^2 its thermal characteristics make it favorable for regions of a ballute seeing the most heating. The IRVE flight demonstrator[4] that is scheduled for launch in 2006 has baselined a ballute that

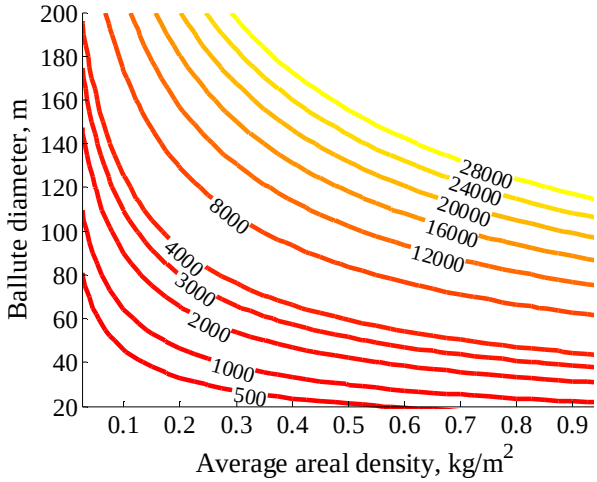

Figure 18. Ballute system mass (kg) at an inflation pressure of 100 Pa.

incorporates a silicone coated Kevlar fabric for the bladder to mitigate tear risk. The remainder of the material stack consists of a dry Kevlar restraint ply, a Kapton gas barrier, and several layers of Nextel cloth for thermal protection. Though areal densities for this material concept are not provided in Reference 4, the entire demonstrator incorporating a three meter ballute is less than 100 kg. The IRVE mission profile, only being a suborbital trajectory, predicts heat rates of about 1 W/cm^2 and dynamic pressures of 600 Pa.

From the prior 9500 kg CEV trajectory results that incorporated ballute jettison one can estimate a required ballute diameter as a function of a limiting heat rate on the ballute. This calculated diameter can then be used to evaluate a required average material density for a specific ballute system mass. Results from this simple analysis are provided in Figure 19. Assuming an entirely thin-film ballute with its corresponding areal density (0.075 kg/m^2) and temperature limits yields a ballute system mass of about 3.5 metric tons or nearly 37% of the assumed entry vehicle mass. For comparison, the thermal protection system for the Apollo Command Module constituted slightly less than 30% of the capsules gross mass[6]. Achieving similar mass fractions for the ballute alone would correspond to system masses of 2.85 and 0.95 metric tons, both of which would require significant improvements in either areal density or temperature limits of the material concepts previously mentioned. The most direct means of improvement in the

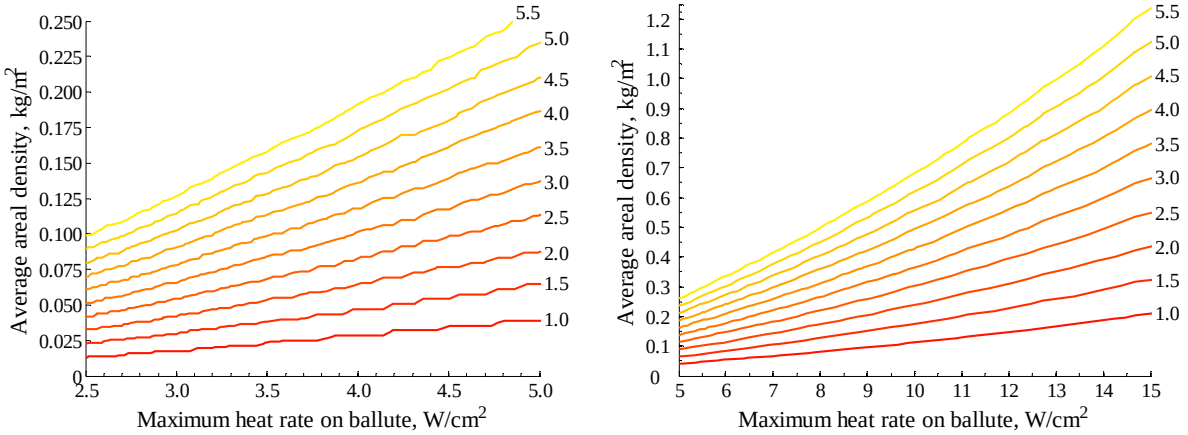

Figure 19. Ballute entry system mass (MT) as a function of maximum ballute heat rate and average areal density for an entry mass of 9.5 MT and an entry velocity of 11.1 km/sec.

mass estimates computed in this investigation are improvements in material areal density and thermal limitations. For example, assuming the same 4.5 W/cm^2 limit as before, a ballute with an areal density of 0.025 kg/m^2 would allow for mass fractions of around 8%.

The same methodology of equating a ballute diameter to a given heat rate constraint and backing out a required areal density was applied to the cargo CEV variants. These results, as a percentage of the entry mass, are provided in Figure 20. It should be mentioned that the lines of ballute system mass fraction represent quadratic least squares regression fits to the full range of entry masses. Of interest is that the plotted trends are observed to hold quite well regardless of entry mass. In other words, for a given heat rate limitation and ballute areal density, the ballute system mass is roughly a fixed percentage of the entry mass. This result further underscores the importance of material properties on ballute system design. That is, if viability is measured by the ballute system mass fraction, than a direct correlation between viability and the material properties of the ballute is evident.

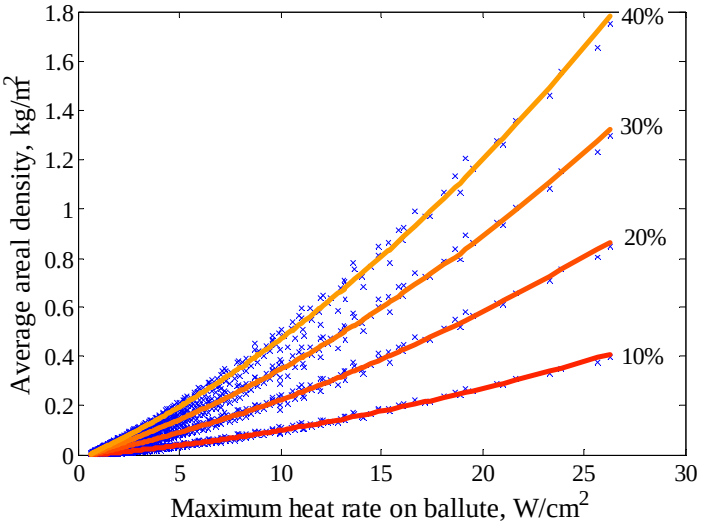

Figure 20. Ballute entry system mass percentages as a function of heat rate limitations and average areal density for an entry velocity of 11.1 km/sec.

IV. Conclusions

This paper focused on analyzing the potential benefits that a clamped ballute entry system can provide to a candidate capsule shaped entry vehicle with a mass of 9500 kg entering Earth's atmosphere at lunar return velocities. For trajectories that retained the ballute, heat rates were observed to vary from 40 W/cm^2 for a 40 m diameter ballute to as low as 2 W/cm^2 for a 200 m diameter ballute. Peak deceleration values were observed to be as low as six g's but generally exceeded seven g's. For larger ballutes in excess of 100 m, dynamic pressures of about 75 Pa were experienced. Minimum deceleration and dynamic pressure both occurred at flight path angles slightly steeper than the overshoot boundary. This phenomenon occurred due to the skipping nature of shallow entries, producing multiple deceleration pulses with the latter one being the strongest. This behavior was mitigated by jettisoning the ballute after a significant velocity decrement. For entries that maintained a zero angle-of-attack after ballute jettison, entry vehicle heat rates were calculated to be within reusable TPS limits of 35 W/cm^2. However, peak deceleration values generally exceed 7.75 g's. Minimization of heat rates, peak g's, and dynamic pressure favored releasing the ballute at an inertial velocity of around 7.8 km/sec. Entries that transitioned to an L/D of 0.3 after ballute release provided further mitigation of heating and deceleration on the CEV. Heat rates as low as 21 W/cm^2 and decelerations as low as four g's were shown to be possible. Reductions in heating and deceleration were attained over a range of ballute diameters, indicating that ballute sizing is primarily driven by the heating constraints of the ballute material. Lastly, variations in entry mass for a cargo variant of the CEV were investigated. From these it was seen that for a heat rate limitation of 4.5 W/cm^2, each metric ton reduction in entry mass allowed for a 10 m reduction in required ballute diameter.

Ballute systems were sized to evaluate technical requirements that improve concept feasibility. Using the trajectory results from the initial part of the study, trends of required average areal density of the ballute versus heat rate limitations for a given ballute system mass were generated. These contours in turn provide guidance as to the technical requirements that a candidate ballute must meet. Mass estimates assuming a thin-film material produced vehicle mass fractions of 37% for the 100 m ballute system alone. However, reducing the areal density by two thirds subsequently reduced the mass fraction to less than 8%, demonstrating the high sensitivity to areal density. Varying entry mass was observed to have little impact on the ballute mass fraction for a given areal density and heating constraint. Material requirements indicate that continued technology development is required for concept viability.

References

[1] Miller, K. L., Gulick, D., Lewis, J., Trochman, B., Stein, J., Lyons, D. T., and Wilmoth, R. G., "Trailng Ballute Aerocapture: Concept and Feasibility Assessment," AIAA Paper 2003-4655, July 2003.

[2] Westhelle, C. H., and Masciarelli, J. P., "Assessment of Aerocapture Flight at Titan Using a Drag-Only Device," AIAA Paper 2003-5389, August 2003.

[3] Graesslin, M., and Schoettle, U., "Flight Performance Evaluation of the Re-Entry Mission IRDT-1," Paper IAF-01-V.3.05, 52nd International Astronautical Congress, Toulouse, France, Oct. 1-5 2001.

[4] Hughes, S. J., Dillman, R. A., Starr, B. R., Stephan, R. A., Lindell, M. C., Player, C. J., and Cheatwood, F. M., "Inflatable Re-entry Vehicle Experiment (IRVE) Design Overview," AIAA Paper 2005-1636, 18th AIAA Aerodynamic Decelerator Systems Technology Conference and Seminar, Munich, Germany, May 23-36, 2005.

[5] Rohrschneider, R. R., and Braun, R. D., "A Survey of Ballute Technology for Aerocapture," Proceedings of the 3rd International Planetary Probe Workshop, Athens, Greece, June, 2005.

[6] "Apollo Program Summary Report: Synopsis of the Apollo Program Activities and Technology for Lunar Exploration," NASA-TM-X-68725, Apr. 1975.

[7] Tran, H. K., Johnson, C. E., Rasky, D. J., Hui, F. C. L., Hsu, M., and Chen, Y. K., "Phenolic Impregnated Carbon Ablators (PICA) for Discovery Class Missions," AIAA Paper 96-1911, 31st AIAA Thermophysics Conference, New Orleans, LA, June 1996.

[8] "NASA's Exploration Systems Architecture Study," NASA-TM-2005-214062, Nov. 2005.

[9] Gnoffo, P. A., and Anderson B. P., "Computational Analysis of Towed Ballute Interactions," AIAA Paper 2002-2997, 8th AIAA/ASME Joint Thermophysics and Heat Transfer Conference, St. Louis, MI, June 2002.

[10] Anderson, B. P., "Computational Continuum and Rarefied Flow Results for Ballute Applications," AIAA Paper 2004-292, 42nd AIAA Aerospace Sciences Meeting and Exhibit, Reno, NV, Jan. 2004.

[11] Graves, C. A. and Harpole, J. C., "Apollo Experience Report – Mission Planning for Apollo Entry," NASA-TN-D-6727, 1972.

[12] Regan, F. J., and Anandakrishnan, S. M., "Flowfield Description," *Dynamics of Atmospheric Re-Entry*, 1st ed., edited by J. S. Przemieniecki, AIAA Education Series, AIAA, Washington DC, 1993, pp. 318-364.
[13] Powell, R. W., et al., "Program to Optimize Simulated Trajectories (POST) Utilization Manual, Volume II, Version 5.2," NASA Langley Research Center, Hampton, VA; Martin Marietta Corporation, Denver, CO, Oct. 1997.
[14] Sutton, K. S., and Graves, Jr., R. A., "A General Stagnation-Point Convective-Heating Equation for Arbitrary Gas Mixtures," NASA TR-R-376, Nov. 1971.
[15] Tauber, M. E., and Sutton, K., "Stagnation-Point Radiative Heating Relations for Earth and Mars Entries," *Journal of Spacecraft and Rockets*, Vol. 28, No. 2, 1991, pp. 40-42.
[16] Richardson, E. H., Munk, M. M., James, B. F., and Moon S. A., "Review of NASA In-Space Propulsion Technology Program Inflatable Decelerator Investments," AIAA Paper 2005-1603, 18th AIAA Aerodynamic Decelerator Systems Technology Conference and Seminar, Munich, Germany, May 23-36, 2005.
[17] Gnoffo, P. A., "Planetary-Entry Gas Dynamics," *Annual Review of Fluid Mechanics*, Vol. 31, pp. 459-494, 1999.
[18] Humble, R. W., Henry, G. N., and Larson, W. J., *Space Propulsion Analysis and Design*, 1st ed. Revised, Space Technology Series, McGraw-Hill, New York, 1995, pp. 272-279.
[19] Brown, G. J., Epp, C., Graves, C., Lingard, J. S., and Darly, M., "Hypercone Inflatable Supersonic Declerator," AIAA Paper 2003-2167, 17th AIAA Aerodynamic Declerator and Systems Technology Conference and Seminar, Monteray, CA, May 19-22, 2003.
[20] Lyons, D., and Johnson, W., "Ballute Aerocapture Trajectories at Neptune," AIAA Paper 2004-5181, AIAA Atmospheric Flight Mechanics Conference and Exhibit, Providence, RI, Aug. 2004.
[21] Kustas, F. M., Rawal, S. P., Willcockson, W. H., Edquist, C. T., Thornton, J. M., and Sandy, C., "Evaluation of High Temperature Multilayer Insulation for Inflatable Ballute," *Journal of Spacecraft and Rockets*, Vol. 38, No. 4, 2001, pp. 630-631.